Reflection and transmission properties of self-similar interfaces

for RIO'99

Kees Wapenaar and Jacob Fokkema

Centre for Technical Geoscience, Delft University of Technology

Abstract

We represent an interface by a self-similar singularity, embedded between two homogeneous half-spaces and we evaluate its frequency-dependent normal incidence reflection and transmission coefficients. For $f \to 0$ the expressions for the coefficients reduce to those for a discrete boundary between two homogeneous half-spaces; for $f \to \infty$ the effect of the embedding half-spaces vanishes. These asymptotic expressions have a relatively simple form and depend on the singularity exponent α.

INTRODUCTION

We parameterize an interface by the following singular function for the P-wave velocity:

$$c(z) = \begin{cases} c_1 |z/z_1|^{\alpha_1} & \text{for } z < 0 \\ c_2 |z/z_2|^{\alpha_2} & \text{for } z > 0, \end{cases} \tag{1}$$

(the mass density will be parameterized as a step-function from ϱ_1 to ϱ_2 throughout this paper). When only one of the parameters α_1 and α_2 is not equal to zero we speak of a one-sided singularity; when both are non-zero the singularity is two-sided. For a two-sided singularity with $\alpha_1 = \alpha_2 = \alpha$ it appears that the function in equation (1) is *self-similar*, according to $c(\beta z) = \beta^\alpha c(z)$, for $\beta > 0$. For $\alpha_1 = \alpha_2 = 0$ this function reduces to the usual step-function.

	$z < 0$ (n=1)	$z > 0$ (n=2)
c_n [m/s]	800	1200
ϱ_n [kg/m^3]	1000	1000
z_n [m]	-5	5
Two-sided: $\alpha_n\ (= \alpha)$	-0.4	-0.4
One-sided: α_n	0	-0.4

Table 1. Parameter values, used in the examples in this paper.

For a two-sided singularity, with parameters α, c_n and z_n as defined in Table 1, the function $c(z)$ as defined by equation (1) is shown in Figure 1a (left figure). We applied a multiscale analysis to this function, following the method described by Mallat and Hwang (1992) and Herrmann (1997). Figure 1b shows the continuous wavelet transform $\check{c}(\sigma, z)$ of this function. In essence this result has been obtained by convolving $c(z)$ with scaled versions of one and the same analyzing wavelet, i.e., with $\frac{1}{\sigma}\psi(\frac{z}{\sigma})$ (this wavelet will be discussed in more detail in a later section). The different traces in Figure 1b correspond to different scales σ. Taking the modulus of the data in Figure 1b and connecting the local maxima from trace to trace, yields the so-called modulus maxima line that is shown in Figure 1c. Figure 1d shows the amplitudes measured along this line, on a log-log scale. The slope of this amplitude-versus-scale (AVS) graph corresponds to the singularity exponent $\alpha = -0.4$ of the self-similar function in Figure 1a (Mallat and Hwang, 1992). Note that when this type of analysis would be applied to a step-function, the slope of the AVS curve would be zero. The AVS behaviour, observed in Figure 1d, corresponds nicely to that of several outliers in real well-logs, as analyzed by Herrmann (1997). Although this 'constant-slope' behaviour is not universal, it makes sense to use functions of the form of equation (1) for the parameterization of composite reflectors. In

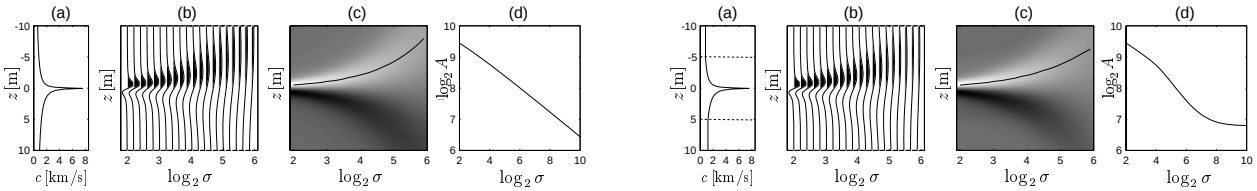

Figure 1: Left figure: (a) Two-sided self-similar velocity function, described by equation (1), with α, c_n and z_n defined in Table 1. (b) Continuous wavelet transform of the velocity function in figure a. (c) Modulus maxima line, obtained from figure b. (d) Amplitude-versus-scale (AVS) curve, measured along the modulus maxima line in figure c. The slope ($\alpha = -0.4$) corresponds to the singularity exponent of the function in figure a. Right figure: Multi-scale analysis of the self-similar velocity function, embedded between two homogeneous half-spaces $z \leq z_1 = -5$m and $z \geq z_2 = 5$m. For small σ the slope of the AVS curve in (d) is constant and again given by $\alpha = -0.4$; for large σ the slope approaches zero, as for a step-function.

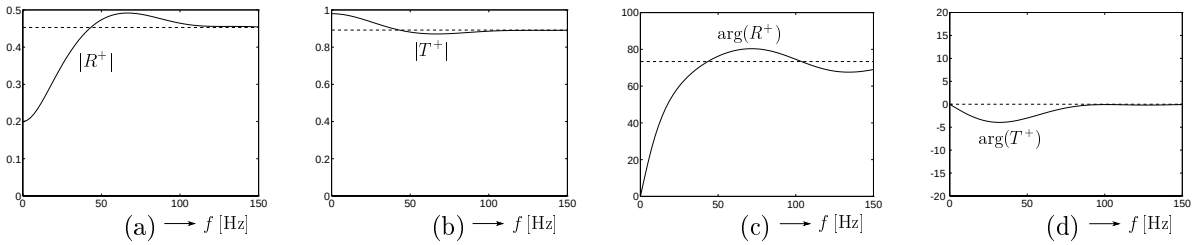

Figure 2: (a,b) Modulus of the reflection and transmission coefficients of the embedded two-sided singularity (solid) and their high-frequency approximations (dashed). (c,d) Idem for the phase.

this paper we will consider the situation in which a self-similar singularity is embedded between two homogeneous half-spaces. A multiscale analysis of such an embedded singularity is shown in the right part of Figure 1. The singular function is defined in the region $z_1 < z < z_2$ with the parameters of Table 1; the velocities of the embedding half-spaces are also given by $c_1 = 800$m/s and $c_2 = 1200$m/s, so that $c(z)$ is continuous at z_1 and z_2. Note that for small scales ($\sigma \to 0$) the AVS curve in Figure 1d (right) approaches that in Figure 1d (left). So in this limit the embedding half-spaces have no effect on the scaling behaviour. For large scales ($\sigma \to \infty$) the AVS curve is nearly constant (as for a step-function), which implies that in this limit the scaling behaviour is fully determined by the embedding half-spaces.

In the following sections we evaluate the normal incidence reflection and transmission properties of this type of self-similar interface. Since the results are exact, they may serve as a reference for approximate expressions for more general situations. For example, Dessing (1997) analyzes the response of another class of scale-dependent reflector models. For a symmetric self-similar singularity (without embedding half-spaces), his results are consistent with the high-frequency expressions in this paper.

For the oblique incidence response no explicit expressions have been found yet (except for $\alpha = 0$ and $\alpha = -\frac{1}{2}$). However, by exploiting the self-similarity property $c(\beta z) = \beta^{\alpha} c(z)$, it is possible to derive self-similarity relations for the angle-dependent reflection and transmission coefficients. A further discussion of these extensions is beyond the scope of this paper.

Reflection and transmission coefficients

The exact reflection and transmission coefficients for a self-similar singularity, embedded between two homogeneous half-spaces, are derived in Wapenaar (1998). Here we consider the embedded two-sided singularity, with α, c_n, ϱ_n and z_n defined in Table 1. In Figure 2 the modulus and phase of R^+ and T^+ are shown as a function of the frequency. The low- and high-frequency limits will be discussed in the next two sections.

Zero-frequency limit

For two-sided as well as one-sided singularities, embedded between two homogeneous half-spaces, the limits for $f \to 0$ of the reflecion and transmission coefficients $R^{\pm}$ and $T^{\pm}$ are given by

$$R^+ = -R^- \to \frac{\varrho_2 c_2 - \varrho_1 c_1}{\varrho_2 c_2 + \varrho_1 c_1}, \qquad T^+ = T^- \to \frac{2\sqrt{\varrho_2 c_2 \varrho_1 c_1}}{\varrho_2 c_2 + \varrho_1 c_1} = \sqrt{1-(R^+)^2}. \tag{2}$$

Note that these coefficients are equal to the flux-normalized coefficients for a discrete boundary between two homogeneous half-spaces, i.e., for the situation in which the velocity and density are described by step-functions. This is consistent with

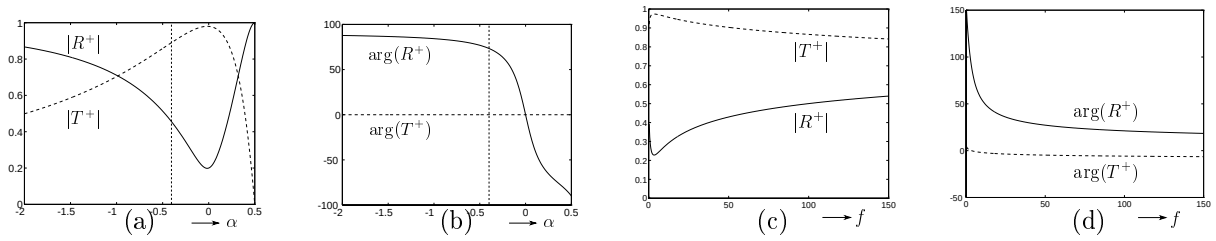

Figure 3: (a,b) High-frequency approximation of the modulus and phase of the reflection coefficient R^+ (solid) and the transmission coefficient T^+ (dashed) of an embedded two-sided singularity. The parameters c_n, ϱ_n and z_n are defined in Table 1. For $\alpha = -0.4$ the moduli and phases correspond to those in Figure 2 for $f \to \infty$. (c,d) Idem for a one-sided singularity with the parameters defined in Table 1.

the multi-scale analysis in Figure 1 (right figure), which revealed that for large σ the embedded self-similar singularity behaves as a step-function (bear in mind that the scale σ is proportional to the wavelength, hence, $\sigma \to \infty$ corresponds to $f \to 0$). For the values of c_n and ϱ_n in Table 1, equation (2) yields $R^+ = -R^- \to 0.2$ and $T^\pm \to \sqrt{0.96}$ (see Figure 2 for $f \to 0$).

High-frequency behaviour for two-sided singularities

For embedded two-sided singularities we take again $\alpha_1 = \alpha_2 = \alpha$ (and $|z_1| = |z_2|$). For this situation the limits for $f \to \infty$ of the reflecion and transmission coefficients $R^\pm$ and $T^\pm$ are given by

$$R^+ = -\{R^-\}^* \to j\left[\frac{\mathrm{e}^{-j\nu\pi}\,\varrho_2 c_2^{2\nu} \;+\; \mathrm{e}^{j\nu\pi}\varrho_1 c_1^{2\nu}}{\varrho_2 c_2^{2\nu} \;+\; \varrho_1 c_1^{2\nu}}\right], \qquad T^+ = T^- \to \frac{2\sin(\nu\pi)\sqrt{\varrho_2 c_2^{2\nu}\,\varrho_1 c_1^{2\nu}}}{\varrho_2 c_2^{2\nu} \;+\; \varrho_1 c_1^{2\nu}}, \tag{3}$$

with $\nu = 1/(2-2\alpha)$ and $\alpha < \frac{1}{2}$. Note that these asymptotic expressions are frequency-*in*dependent. The factor j corresponds to a Hilbert transform in the time domain. For c_n, ϱ_n and z_n as defined in Table 1 and *variable* α, the modulus and phase of the high-frequency reflection and transmission coefficients R^+ and T^+ are shown in Figures 3a and b. For $\alpha = -0.4$ we have $|R^\pm| \to 0.4528$, $\arg(R^+) \to 73.37^o$, $\arg(R^-) \to 106.63^o$, $|T^\pm| \to 0.8916$, $\arg(T^\pm) = 0^o$. These values (except $\arg(R^-)$) are represented by the dashed lines in Figure 2. The coefficients in equation (3) are equal to the exact coefficients for a two-sided self-similar function described by equation (1), (i.e., without the embedding homogeneous half-spaces). This is consistent with the multi-scale analysis in Figure 1 (right figure), which revealed that for small σ the embedding half-spaces have no effect on the scaling behaviour of the singularity (bear in mind that $\sigma \to 0$ corresponds to $f \to \infty$). At this point it is useful to give a quantitative interpretation of the scales σ along the horizontal axes in these figures. As we mentioned in the introduction, the multiscale analysis involves a convolution with a scaled wavelet $\frac{1}{\sigma}\psi(\frac{z}{\sigma})$. The wavelet that was used in Figure 1 is the derivative of a Gaussian, defined as

$$\psi\Big(\frac{z}{\sigma}\Big) = \frac{\partial}{\partial z}\left[\frac{\exp\big[-(\frac{z}{2\sigma\Delta z})^2\big]}{2\sqrt{\pi}}\right], \tag{4}$$

with $\Delta z = 0.1$ m. The Fourier transform of this wavelet is $j(k\sigma\Delta z)\exp[-(k\sigma\Delta z)^2]$ and reaches its maximum at $k_0 = 1/(\sigma\Delta z\sqrt{2})$. Hence, the effective wavelength of the analyzing wavelet is given by $\lambda_{\mathrm{eff}} = 2\pi/k_0 = 2\sqrt{2}\,\pi\sigma\Delta z$, from which we derive that $\log_2\sigma = \{2,\ 4,\ 6,\ 8,\ 10\}$ corresponds to $\lambda_{\mathrm{eff}} = \{3.5,\ 14,\ 57,\ 228,\ 910\}$ m. Unfortunately these wavelengths can not be uniquely related to seismic frequencies, since the velocity is not constant. Using an effective velocity c_{eff} we define the corresponding effective seismic frequency as $f_{\mathrm{eff}} = \frac{c_{\mathrm{eff}}}{\lambda_{\mathrm{eff}}}$. Choosing (quite arbitrary) $c_{\mathrm{eff}} = 2000$ m/s, we thus find that the aformentioned range of scales corresponds to $f_{\mathrm{eff}} = \{570,\ 142,\ 34,\ 9,\ 2.2\}$ Hz. Hence, the scales $\log_2\sigma = 4$ to $\log_2\sigma = 8$ roughly correspond to the seismic scale range. In Figures 1d (left and right) we observe that the AVS curves of the velocity functions in Figures 1a (left and right) match very accurately for scales smaller than the seismic scales; within the seismic scale range they follow a similar trend and for larger scales they are completely different. Hence, the high-frequency approximations given by equation (3) are very accurate for frequencies above the seismic frequency range. How well they perform within the seismic frequency range will be investigated with an example in a later section.

High-frequency behaviour for one-sided singularities

For embedded one-sided singularities we take $\alpha_1 = 0$ and $\alpha_2 \neq 0$. For this situation the limits for $f \to \infty$ of the reflecion and transmission coefficients $R^\pm$ and $T^\pm$ are given by

$$R^+ \;\to\; \frac{\frac{\Gamma(\nu)}{\Gamma(1-\nu)}(j\omega\nu|z_2|)^{1-2\nu}\varrho_2 c_2^{2\nu} - \varrho_1 c_1}{\frac{\Gamma(\nu)}{\Gamma(1-\nu)}(j\omega\nu|z_2|)^{1-2\nu}\varrho_2 c_2^{2\nu} + \varrho_1 c_1}, \qquad R^- \to \frac{-\frac{\Gamma(\nu)}{\Gamma(1-\nu)}(\omega\nu|z_2|)^{1-2\nu}\varrho_2 c_2^{2\nu} + j^{1-2\nu}\varrho_1 c_1}{\frac{\Gamma(\nu)}{\Gamma(1-\nu)}(j\omega\nu|z_2|)^{1-2\nu}\varrho_2 c_2^{2\nu} + \varrho_1 c_1}, \tag{5}$$

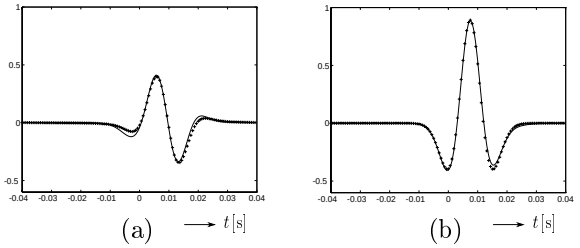

Figure 4: Reflection (a) and transmission (b) responses of the embedded two-sided singularity (solid) and their high-frequency approximations (+).

$$T^{\pm} \quad \rightarrow \quad \frac{\frac{2\sqrt{\pi}}{\Gamma(1-\nu)}\sqrt{(j\omega\nu|z_2|)^{1-2\nu}\,\varrho_2 c_2^{2\nu}\,\varrho_1 c_1}}{\frac{\Gamma(\nu)}{\Gamma(1-\nu)}(j\omega\nu|z_2|)^{1-2\nu}\,\varrho_2 c_2^{2\nu} + \varrho_1 c_1}, \tag{6}$$

with $\omega = 2\pi f$, $\nu = 1/(2-2\alpha_2)$ and $\alpha_2 < \frac{1}{2}$. Note that these asymptotic expressions are frequency-dependent, unlike the coefficients in equation (3) for the two-sided singularity. The factors $(j\omega)^{1-2\nu}$ correspond to a fractional differentiation or integration in the time domain for negative and positive α_2, respectively.
For α_2, c_n, ϱ_n and z_n as defined in Table 1, the modulus and phase of the high-frequency reflection and transmission coefficients R^+ and T^+ are shown in Figure 3c and d.

Reflection and transmission responses

In this section we consider the time-domain reflection and transmission responses of the embedded two-sided singularity shown in Figure 1a (right figure). For the downgoing incident wave field we choose a Ricker wavelet, defined by $s_R(t) = (1-2\pi^2 f_0^2 t^2)\,\mathrm{e}^{-\pi^2 f_0^2 t^2}$, with $f_0 = 50$Hz. The Fourier transform of this wavelet is $S_R(f) = \frac{2}{\sqrt{\pi}}\frac{f^2}{f_0^3}\,\mathrm{e}^{-f^2/f_0^2}$. Multiplying this spectrum with the exact complex reflection and transmission coefficients of Figure 2 and transforming the results back to the time-domain yields the reflection and transmission responses, shown by the solid lines in Figure 4. Note that in the reflection response a significant phase distortion of the Ricker wavelet is observed, in agreement with Figure 2c. The transmission response, on the other hand, has undergone nearly no phase distortion, in agreement with Figure 2d. Figure 4 also shows the high-frequency approximations of the reflection and transmission responses, denoted by the crosses (+). These responses have been obtained using the asymptotic reflection and transmission coefficients of Figures 3a and b (for $\alpha = -0.4$). Note that the main features of the exact responses are reasonably well reproduced by these high-frequency approximations.

Conclusions

We have introduced a scale-dependent interface in which a self-similar singularity is embedded between two homogeneous half-spaces. A multiscale analysis revealed that for large scales ($\sigma \rightarrow \infty$) this interface is indistinguishable from the usual step-function whereas for small scales ($\sigma \rightarrow 0$) the scaling behaviour is dominated by the singularity. We have presented analytical results for the normal incidence reflection and transmission coefficients of this interface. These coefficients appear to be frequency-dependent. For small frequencies ($f \rightarrow 0$) these coefficients reduce to the well-known coefficients of a step-function interface, whereas for large frequencies ($f \rightarrow \infty$) the coefficients are equal to those of a singular function without the embedding half-spaces. For two-sided singularities these asymptotic coefficients are frequency-*in*dependent; the factor j in the expression for the reflection coefficient corresponds to a Hilbert transform in the time domain. For one-sided singularities the asymptotic coefficients are frequency-dependent; the factors $(j\omega)^{1-2\nu}$ correspond to a fractional differentiation/integration in the time domain.
Throughout this paper we have restricted ourselves to the normal incidence responses of one particular form of a self-similar interface. Since the results are exact, they may serve as a reference for approximate expressions that can handle more general situations.

Acknowledgements

The authors would like to thank Frank Dessing and Jeroen Goudswaard for the fruitful discussions and for carrying out the multiscale analyses of the singular functions. This work is financially supported by the Dutch Technology Foundation.

REFERENCES

F. J. Dessing. *A wavelet transform approach to seismic processing*. PhD thesis, Delft University of Technology, 1997.
F. J. Herrmann. *A scaling medium representation*. PhD thesis, Delft University of Technology, 1997.
S. G. Mallat and W. L. Hwang. Singularity detection and processing with wavelets. *IEEE Tr. Inf. Th*, 38(2):617–643, 1992.
C. P. A. Wapenaar. Seismic reflection and transmission coefficients of a self-similar interface. *G. J. I.*, 135:585–594, 1998.